Biosensors and Bioelectronics 140 (2019) 111271

Contents lists available at ScienceDirect

Biosensors and Bioelectronics

journal homepage: www.elsevier.com/locate/bios

Porous carbon supported nanoceria derived from one step *in situ* pyrolysis of Jerusalem artichoke stalk for functionalization of solution-gated graphene transistors for real-time detection of lactic acid from cancer cell metabolism

Yulong Bi[a,1], Lihui Ye[a,1], Yu Mao[a], Lu Wang[a,*], Hao Qu[a,b,**], Jian Liu[a,***], Lei Zheng[a,****]

[a] School of Food and Biological Engineering, Hefei University of Technology, Hefei, Anhui, 230009, China
[b] CAS Key Laboratory of Bio-inspired Materials and Interfacial Science, Technical Institute of Physics and Chemistry, Chinese Academy of Sciences, Beijing, 100190, China

ARTICLE INFO

Keywords:
Porous carbon
Nanoceria
Biomass pyrolysis
Solution-gated graphene transistors
Lactic acid

ABSTRACT

Effective detection of biomarkers for tumor cells has been the focus of attention. In this work, we have successfully fabricated a highly sensitive sensor based on solution-gated graphene transistors (SGGT) for detecting lactic acid content accumulated in tumor cells through their glycolysis metabolism. The sensing mechanism of the lactic acid sensor is attributed to electrochemical catalysis of H_2O_2 produced by the oxidation of lactic acid by lactate oxidase near the gate electrode. The key component of the sensor is the functionalization of porous carbon loaded with ceria nanoparticles derived from a novel one step *in situ* pyrolysis of pretreated Jerusalem artichoke stalk, which significantly improved the sensor sensitivity, i.e. a detection limit as low as 300 nM and linear range from 3 μM to 300 μM. The optimized lactic acid sensor has successfully applied to the detection of lactic acid in practical cell culture samples with high credibility. The SGGT-based lactic acid biosensor shows great potential for the application in tumor microenvironment due to its superior biocompatibility and accuracy.

1. Introduction

Cancer has become the second leading threat to human health and the number of people die of cancers is still growing rapidly. It has been reported that from 2006 to 2016 the number of cancer deaths increased by 17.8%, from 7.58 million to 8.93 million (GBD, 2016 Disease and Injury Incidence and Prevalence Collaborators, 2017). Early diagnosis and treatment of cancers has been regarded as an effective approach for prolonging the survival time and even complete cure of patients.

As is known to all, there are two main metabolic pathways of intracellular carbohydrate metabolism, i.e. aerobic respiration and glycolysis. In normal cells, oxidative phosphorylation of glucose is usually the main metabolic mode. On contrary, when cell carcinogenesis occurs, it has been reported that tumor cells bypass the pathway of aerobic metabolism and conduct glycolysis for energy supply (Xie et al., 2014). This process accumulates large amounts of lactic acid around the tumor tissue. For example, the lactate concentrations in Hepato Cellular Carcinoma (HCC) biopsies were around 20 mM (Chao et al., 2016), leading to the acidic microenvironment of tumor. Therefore, rapid and sensitive detection of lactic acid in biological system offers a potential approach for the routine analysis and diagnosis of tumor cells.

Various analytical methods for measuring lactic acid have been developed, including high performance liquid chromatography (HPLC) (Ross et al., 2010), mass spectroscopy (MS) (Tserng et al., 1984), electrochemical detection (Hernández-Ibáñez et al., 2016), and transistor-based sensing (Khodagholy et al., 2012). However, these methods have some limitations in practical applications. For example, they generally require large equipment, complex operation, and excessive maintenance costs. And most importantly, these analytical methods take long time for final results and hence do not meet the need for quick, continuous and on-site determination of lactic acid. A transistor-based electrochemical sensor have shown promising applications in a variety of chemical and biological sensors (Lin and Yan, 2012). Advantages of transistor-based electrochemical sensors include high sensitivity, low cost, ease of manufacture, flexibility and biocompatibility (Novoselov et al., 2004). Transistor-based sensors are a combination of

* Corresponding author. School of Food and Biological Engineering, Hefei University of Technology, Hefei, 230009, Anhui, China.
** Corresponding author. School of Food and Biological Engineering, Hefei University of Technology, Hefei, Anhui, 230009, China.
*** Corresponding author.
**** Corresponding author.
E-mail addresses: wanglu@hfut.edu.cn (L. Wang), quhao@hfut.edu.cn (H. Qu), liujian509@hfut.edu.cn (J. Liu), lei.zheng@aliyun.com (L. Zheng).
[1] Yulong Bi and Lihui Ye contributed equally to this work.

https://doi.org/10.1016/j.bios.2019.04.039
Received 22 January 2019; Received in revised form 19 April 2019; Accepted 19 April 2019
Available online 10 May 2019
0956-5663/

a sensor and an amplifier that can cause significant changes in channel current due to small potential changes on the surface of the gate electrode. Among them, solution-gated graphene field effect transistor (SGGT) is a transistor-based sensor with a graphene channel that operates in solution and has been widely applied across many fields (Liu et al., 2012; Rumyantsev et al., 2012). Its main feature, ultra-sensitivity (usually assessed by the detection limit, i.e. the minimum concentration of the analyte can be distinguished from the blank value) originates from its inherent amplification function, namely the tiny voltage applied by the electrolyte/graphene interface on the gate surface (ie, electric double layer EDL in Fig. S1) to regulate the channel current between the source and drain.

To further enhance the performance of SGGT based sensors, people have applied many types of functionalization to the gate electrode or the channel, such as noble metals (e.g. Pt (Zhai et al., 2013), Au (Hammock et al., 2013)), and transition-metal oxides (e.g. Fe_3O_4 (Miao et al., 2017), Co_3O_4 (Xiong et al., 2018), CeO_2 (Liu et al., 2015)). Among them, ceria (CeO_2) nanoparticles have received broad attention in electrochemical applications because of their superior electrocatalytic properties, excellent catalytic stability, low cost and good biocompatibility (Montini et al., 2016). It has been reported that the approach for immobilization of functionalizing materials also plays a significant role (Zhou and Hartmann, 2013; Zhang et al., 2017).

Recently, porous carbon materials with outstanding electrical conductivity and chemical stability, high surface area, and loading capacity have received significant attention across many fields, including electrochemical capacitors (Hou et al., 2015), lithium-ion batteries (Gaddam et al., 2016; Zhou et al., 2017), catalysis (Han et al., 2014), drug delivery (Huang and Lovell, 2016), etc. Since porous carbon materials integrate the merits of a carbonaceous composition and porous features, they show superior properties compared with traditional porous silica and other carbon-based nanomaterials. Current syntheses can be categorized as hard-template or soft-template methods, both require well supplied carbon precursor resources (Wang et al., 2016).

Biomass is the most abundant and renewable carbon sources on the earth and has optimal structure of carbon materials through evolution (Saikat et al., 2014). It has been regarded as a well suitable precursor for porous carbons and has already been widely applied for their fabrication because of its low cost, eco-friendly features (Pode, 2016). The simplest approach to obtain porous carbons from biomass is pyrolysis of native materials under low oxygen environment through which porous carbon matrix naturally forms based on the original porous structure of biomass materials upon carbonization (Zhong et al., 2017; Veerakumar et al., 2016). The generated porous carbons are reported to have many unique advantages. For example, the large surface area and high porosity of biomass derived porous carbon make it very promising for catalytic applications (Chen et al., 2018).

Jerusalem artichoke is a kind of important cash and energy crop with high tolerance to barren and harsh environment (Long et al., 2016). So, the planting area of Jerusalem artichoke is growing every year. The stalk of Jerusalem artichoke generally grows up to 1–3 m, producing a large amount of biomass resources. Unlike other common agricultural biomass, Jerusalem artichoke stalk contains a substantial portion of lignin. Besides, it has been reported that Jerusalem artichoke stalk has honeycomb like porous structures that may retain during pyrolysis process, yielding high-quality porous carbon materials (Lei et al., 2015).

The key factor for functionalization of SGGT based sensors lies in how to effectively load the ceria nanoparticles into porous carbon backbones. In this paper, we report a novel “one-step” approach for production of 3D porous carbon supported ceria nanoparticles (JACM/CeO_2NPs) from *in situ* pyrolysis of cerium nitrate pretreated Jerusalem artichoke straw biomass. We found that the nanocomposites of JACM/CeO_2NPs exhibited exceptional capability of electrochemical catalytic oxidation of H_2O_2. Incorporated with lactic acid oxidase, the nanocomposites of JACM/CeO_2NPs were used for modification of the gate electrode of SGGT. This functionalization greatly improved the sensitivity of the optimized SGGT sensor for lactic acid, showing a detection limit as low as 300 nM, far beyond the sensitivity required for practical applications. In the end, we also demonstrated that the modified SGGT sensor was ready for distinguishing cancer cells from normal cells judging from the lactic acid generated by the metabolism of cancer cells. Considering the availability of biomass materials and the convenience of the one-step approach, we believe JACM/CeO_2NPs provides a highly potential functionalization material for improving the performance of SGGT sensors for a wide application in diagnosis of disease-related biomarkers and healthcare monitoring.

2. Materials and methods

2.1. Materials

Jerusalem artichoke stalk (JA) was collected from east of Anhui province, China. DL-lactic acid (LA), phosphate buffered saline (10 × PBS, a mixed solution of 80 mM Na_2HPO_4, 1.36 M NaCl, 20 mM KH_2PO_4 and 26 mM KCl, with pH = 7.2) were purchased from Sangon (Shanghai, China). Cerium nitrate hexahydrate ($Ce(NO_3)_3{\cdot}6H_2O$) was purchased from Macklin (Shanghai, China). Lactate oxidase (LOD) (9.5 mg/mL, 106 U/mg) was purchased from Yuanye biology (Shanghai, China). Hydrogen peroxide (H_2O_2), chitosan (CS), potassium chloride (KCl), potassium hydroxide, sodium nitrate ($NaNO_3$), sodium sulfate (Na_2SO_4), sodium chloride (NaCl), glycine (Gly), D-glucose (Glu), urea were purchased from Sinopharm (Shanghai, China). Dulbecco's modified Eagle's medium (DMEM) with high glucose, 110 mg/L sodium pyruvate were purchased from Gibco (Auckland, New Zealand). The lactic acid kit for determination of lactic acid concentration was purchased in Jiancheng (Nanjing, China). Ultrapure deionized (DI) water was produced by a Milli-Q system (18.2 MΩ, Millipore, Bedford, MA, USA). All the reagents were used without further purification.

2.2. In situ synthesis of porous carbon supported nanoceria (JACM/CeO_2NPs)

As shown in Fig. 3a After washing, drying, and fine-grinding, Jerusalem artichoke stalk was pretreated with 0.5 L cerium nitrate hexahydrate (2 mM) in a beaker with magnetic stirring for 20 min. After saturation, 1.5 mL hydrogen peroxide and 7.5 mL of ammonia were added to the beaker, followed by 1.5 g cetyltrimethyl ammonium bromide (CTAB) for better dispers ion of particles. After 1 h, the suspension was filtered to remove large sediments and then dried at 60 °C overnight. Pipe furnace was used for pyrolysis of the above dried materials. The pyrolysis was performed under nitrogen atmosphere with heating rate of 10 °C/min, insulation heat up to 800 °C for 2 h. The biochar was grounded, sieved, and washed in 5 M KOH solution for 12 h. Finally, the cathartic cleaning solution was neutral and remained to be used.

2.3. Preparation of JACM/CeO_2NPs/LOD/CS modified electrode for lactic acid detection

The SGGT device was designed as shown in Fig. 3b Chitosan (4 mg) was completely dissolved in 20 mL of 1% acetic acid solution. The above-mentioned *in situ* synthesized nanocomposites of JACM/CeO_2NPs were added to the prepared chitosan solution with a final concentration of 1 mg/mL, and ultrasonically dispersed for 2 h. We applied each 10 μL of this mixed suspension to the bare gate electrode. The gate electrode was naturally air-dried. Then, 5 μL of LOD solution was added to 5 μL of the chitosan solution with careful mixing to avoid bubbles. The LOD in chitosan solution was added drop wisely to the above dried JACM/CeO_2NPs/CS modified gate electrode. The electrode was then dried at 4 °C.

2.4. Modified material characterization

Crystallographic structures of the JACM/CeO_2NPs samples was obtained from X-ray diffraction (XRD) measurement by X'Pert PRO MPD (1.6 kW) with CuKα radiation (λ = 1.5405 Å) in a 2θ range from 10 to 60° with scanning rate of 1°/min. JACM and JACM/CeO_2NPs were characterized by microscopic confocal laser Raman spectroscopy (633 nm, HR Evolution) for the degree of graphitization of porous carbon. JACM and JACM/CeO_2NPs were also characterized by ESCALAB 250Xi X-ray photoelectron spectroscopy (XPS) to demonstrate that cerium oxide was successfully supported on biomass carbon. Sample morphology was determined by a SU8020 field emission scanning electron microscopy (FE-SEM).

2.5. Electrochemical measurement

The electrochemical properties of the bare and modified electrodes were characterized by the CHI650D electrochemical workstation (Shanghai CH Instruments Inc., China). All electrodes were rinsed with deionized water before test to remove floating dust from the surface. We used a saturated calomel electrode (SCE) as the reference electrode, and a Pt wire as the counter electrode. Three electrodes composed of bare Au gate, JACM/CeO_2NPs/CS and JACM/CeO_2NPs/LOD/CS respectively were tested. Cyclic voltammograms (CV) were performed at 1 × PBS (a mixed solution of 80 mM Na_2HPO_4, 1.36 M NaCl, 20 mM KH_2PO_4 and 26 mM KCl with pH 7.4) at a scan rate of 50 mV/s with a scan range of 0–0.8 V. Electrochemical impedance spectroscopy (EIS) was performed on bare Au gate, JACM/CeO_2NPs/CS/Au and JACM/CeO_2NPs/LOD/CS/Au in 0.1 mM KCl solution containing 5.0 mM $[Fe(CN)_6]^{3-/4-}$ and the frequency range from 0.1 to 10^5 Hz, the potential used is 0.2 V (Zheng et al., 2016). The curve was recorded at certain applied potentials under continuous stir.

All devices were immersed in 1 × PBS for 15 min before lactic acid was detected in real time and rinsed thoroughly. All SGGT-based sensors for lactic acid detection, including source, drain and gate electrodes, were all immersed in a beaker containing 10 mL of 1 × PBS solution. The source and drain, and the gate are connected to two source meters (Keithley 2400), respectively. The gate voltage (V_G) and source-drain voltage (V_{DS}) were controlled by Labview program. Different concentrations of lactic acid were then added to the PBS. To get consecutive different I_{DS} responses. Lactic acid was detected under a fixed V_{DS} = 0.05 V and a gate voltage V_G = + 0.7 V. Including the transfer curve (I_{DS}-V_G, measuring the channel current between the source and drain as a function of V_G at a fixed V_{DS} = 0.05 V) and the channel current versus time curve (I_{DS}-t, at a constant The change of I_{DS} response generated by each sensor for different concentrations of lactic acid added with time was measured under V_G = + 0.7 V and V_{DS} = 0.05 V.

2.6. Cell cultivation process

The human hepatoma HepG2 cell line seeded at a density of 4×10^5 cells/well in 35 mm dishes, and were maintained as subconfluent cultures in DMEM supplemented with 25 mM glucose, 10% Fetal Bovine Serum (FBS), 1 mM sodium pyruvate, 100 μg/mL penicillin and 100 μg/mL streptomycin (medium A). Cells culture and further analyses were conducted at 37 °C under an atmosphere of 5% CO_2 and 95% air. The human cervical cancer Hela cell line and the lung cancer cell A549 cell line were provided by the University of Science and Technology of China (Hefei, China), and cultured the same way. The experimental incubations were terminated by collecting the incubation medium and washing the cells with 1 mL 1 × PBS.

2.7. Standard assay for lactic acid concentration in the cell medium

With Nicotinamide adenine dinucleotide (NDA) as the hydrogen acceptor, Lactate dehydrogenase (LDH) catalyzes the dehydrogenation of lactate to produce pyruvate, which converts NAD to NADH. With NDA as the hydrogen acceptor, LDH catalyzes the dehydrogenation of lactate to produce pyruvate, which converts NAD to NADH. The hydrogenation of phenazine methosulfate (PMS) reduces the nitrotetrazolium blue chloride (NBT) to a purple color, and the absorbance of the colorant is linear with the lactic acid content at 530 nm.

According to the kit operation steps, the lactic acid content is obtained according to the formula:

$$C = \frac{OD_2 - OD_0}{OD_1 - OD_0} \quad (1)$$

where C is the lactic acid concentration (mM), OD_0 is the absorbance of the blank medium at 530 nm, OD_1 is the absorbance value of lactic acid reference at 530 nm,OD_2 is the absorbance of cell culture medium at 530 nm. All OD530 values were detected by microplate reader.

3. Results and discussion

3.1. Characterization of nanoceria loaded porous carbon nanocomposites

The morphology the JAME/CeO_2NPs by FE-SEM are shown in Fig. 1d and e. It can be clearly seen that the carbon derived from pyrolysis of Jerusalem artichoke stalk (before loading nanoceria) shows a honeycomb like porous structure, very suitable for nanoceria supporting matrix. Pretreating Jerusalem artichoke stalk with cerium nitrate as the precursor, we found that nanoceria was successfully synthesized on the surface of the porous carbon walls by the one step *in situ* pyrolysis method.

The X-ray diffraction (XRD) pattern of JACM and JACM/CeO_2NPs as shown in Fig. 1a demonstrates that there are 2θ notable differences between 10 and 60°. Compared to JACM XRD spectrum, JACM/CeO_2NPs XRD spectrum shows absorption peak at 28.6° and 33.1° and 47.5° and 56.4° and 59.2°, corresponding to the CeO_2 (111) (200) (220) (311) (222) characteristic peak (Deshpande et al., 2005). This clearly indicates the presence of CeO_2 nanoparticles in the pore structure of JACM. Fig. 1b shows the microconfocal laser Raman spectrum of JACM and JACM/CeO_2NPs. It can be seen from the figure that there were obvious absorption peaks around 1300 cm^{-1} and 1580 cm^{-1}. The D and G absorption peak intensity ratio of JACM was I_D/I_G = 0.92, while that of JACM/CeO_2NPs was I_D/I_G = 1.06, indicating that the graphitization degree of JACM was higher than that of JACM/CeO_2NPs. Because the D peak represents a defect in the C atomic lattice, and the G peak represents an in-plane stretching vibration of the C atom sp^2 hybridization. Due to the addition of CeO_2, the oxygen of CeO_2 may lead to partial oxidation of graphitized carbon during carbonization. This leads to the transformation of the C atom from the G peak sp^2 to the D peak sp^3 (Ferrari, 2007). The X-ray photoelectron energy spectrum (XPS) of JACM and JACM/CeO_2NPs is shown in Fig. 1c, which indicates that both materials contain biomass porous carbon materials. Therefore, it is obvious that the absorption peaks of C and O atoms can be found from the figure. The absorption peaks of Ce3d (Bêche et al., 2008) appear in the XPS map displayed by JACM/CeO_2NPs, so it indicates that the composite material synthesized by the *in situ* synthesis method contains CeO_2.

Fig. 2d and e shows the morphology of the gate electrode surface we modified. As can be seen from the figure, the surface area of the gate electrode was increased due to the addition of porous carbon of biomass. In this way, more reaction area is increased, and the catalytic efficiency of CeO_2 and LOD is improved. Fig. 2e is a partial magnification of Fig. 2d, which shows that the electrode surface was covered by chitosan film, and the lactic acid oxidase was also encased on the chitosan, being close to the electrode surface. Therefore, it has been validated that chitosan can serve as a good medium for fixing JACM/CeO_2NPs and LOD firmly on the electrode surface during the modification process.

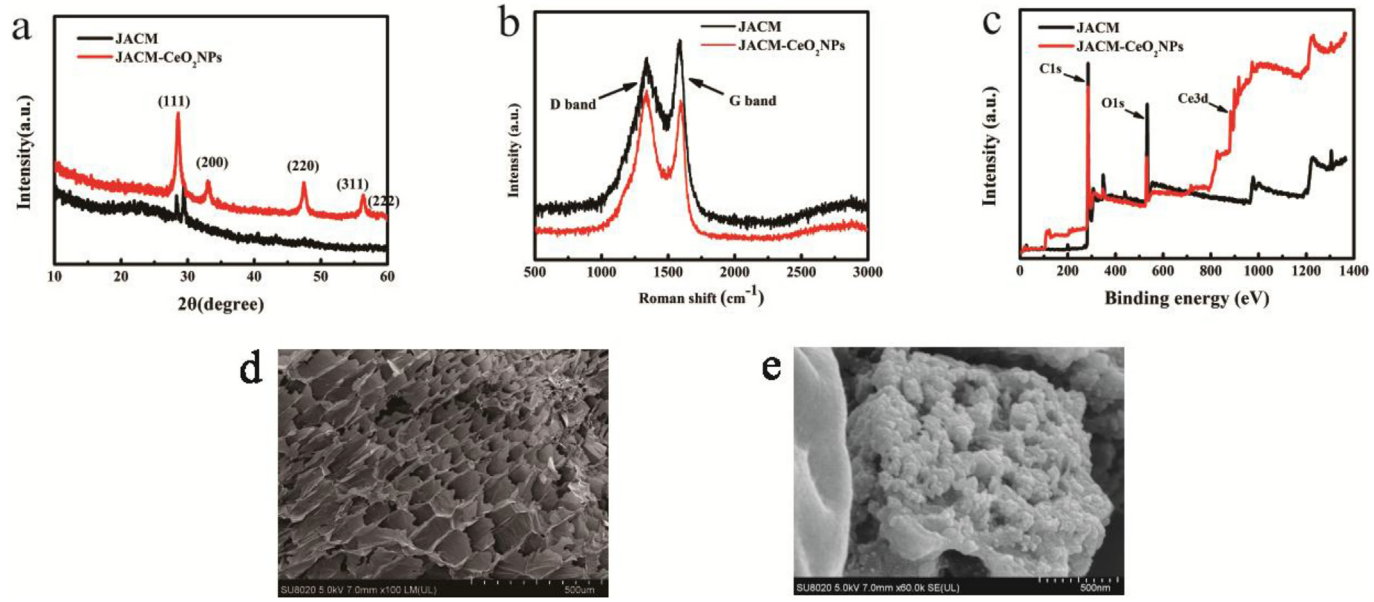

Fig. 1. Functional composite material characterization of JACM and JACM/CeO_2NPs. (a)XRD (b)Raman (c)XPS. And the FE-SEM image of (d) biomass derived mesoporous carbon (before loading). (e) biomass derived porous carbon loading CeO_2 nanoparticles.

3.2. Electrochemical characteristics of JACM/CeO_2NPs/LOD/CS modified electrode

In order to evaluate the catalytic performance of JACM/CeO_2NPs/LOD/CS modified gate electrode, cyclic voltammetry (CV) was used to characterize the electrochemical catalytic capacity of functional composite electrode to H_2O_2. The results are shown in Fig. 2a and we found that the CV oxidation peak of 10 mM H_2O_2 by the JACM/CeO_2NPs modified by Au electrode was 10 times higher than that of bare Au gate, indicating that the modification of JACM/CeO_2NPs significantly enhanced the electrocatalytic oxidation activity of Au gate electrode to H_2O_2. The current peak of the JACM/CeO_2NPs/LOD/CS/Au electrode in Fig. 2a is smaller than that of the JACM/CeO_2NPs/CS/Au electrode. The possible reason is that the electrode impedance increases after the addition of LOD, reducing the electron transfer rate of the electrode (as shown in Fig. 2c).

We have performed additional CV measurements on the three electrodes in PBS buffer without H_2O_2 and found clear Au reduction peaks at 0.3–0.6 V as shown in Fig. S7, similar to the results in (Nagaraj et al., 2015). However, the reduction peak disappeared after the addition of H_2O_2 (see Fig. 2a and b). When the CV characteristics of H_2O_2 are detected in the PBS solution, H_2O_2 exhibit an irreversible reduction process, which has a more significant reduction peak at about −0.4 V (Shan et al., 2010; Zhang et al., 2013). We believe the possible reason

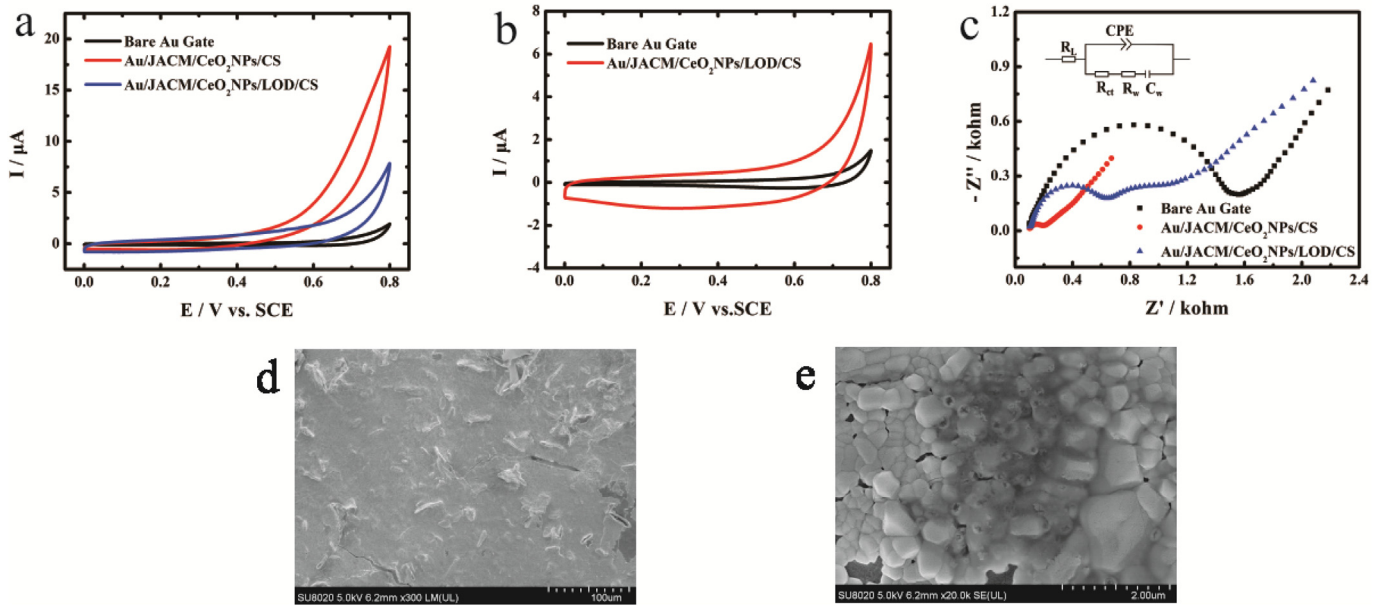

Fig. 2. Characterization of electrochemical properties of functional composite materia (JACM and JACM/CeO_2NPs). (a)The cyclic voltammogram (CV) of the modified electrode in 10 mM H_2O_2 in 1 × PBS (pH = 7.4), scanning rate 50 mV/s (0–0.8 V). (b) The cyclic voltammogram (CV) of the modified electrode in 10 mM lactic acid in 1 × PBS (pH = 7.4), scanning rate 50 mV/s (0–0.8 V). (c) Electrochemical impedance spectroscopy (EIS) of modified electrode obtained in 0.1 mM KCl solution containing 5.0 mM $[Fe(CN)_6]^{3-/4-}$ and the frequency range from 0.1 to 10^5 Hz, the DC voltage used is 0.2 V and the amplitude of 0.001 V. And the FE-SEM image of (d) JACM/CeO_2NPs/LOD/CS modified electrode surface. (e) a larger version of figure.

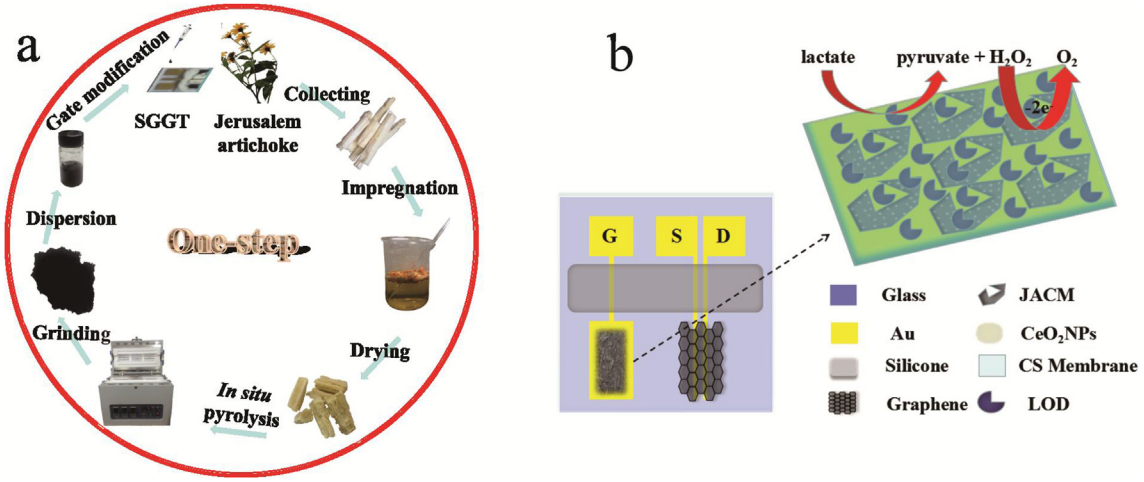

Fig. 3. (a) The schematic of the one-step and sustainable approach for preparing nanoceria loaded porous carbon through *in situ* pyrolysis of pretreated Jerusalem artichoke stalk. (b) The schematic diagram of a solution-gated graphene transistor (SGGT). D, S, G represents the drain, source and gate electrode, respectively. The oxidation of lactic acid occurs at the Au/JACM/CeO_2NPs/LOD/CS modified gate electrode.

for the missing Au reduction peak is that the reduction peak of the Au electrode may have been covered by the irreversible reduction process of H_2O_2. This result is also consistent with the results reported in previous literature (Zhang et al., 2015; Xiong et al., 2018).

We also tested the electrochemical properties of the JACM/CeO_2NPs/LOD/CS modified electrode to 10 mM lactic acid as shown in Fig. 2b, which also indicated a significantly enhanced electrocatalytic performance of the modified electrode.

When we studied the charge transfer of the electrodes, the three electrodes were independently tested by EIS, and the results are shown in Fig. 2c. First, we fit the equivalent circuit diagram (illustrated in Fig. 2c) based on the actual condition (which also contains electrode polarization and concentration polarization). The interpretation of the elements in the equivalent circuit is as follows. R_L is the resistance of the solution between the reference electrode and the working electrode. CPE is a constant phase angle component associated with an electric double layer capacitor. R_{ct} is the charge transfer resistance of the electrode. R_w is the solid phase diffusion of a Warburg resistor. And C_w is the solid phase diffusion of a Warburg capacitor.

We can see from the figure that the Nyquist plot of the three electrodes show a clear semicircle at higher frequencies. The size of the semicircle yields the value of R_{ct} (Chen et al., 2005). Among the three electrodes, the R_{ct} value of the bare Au electrode is about 1500 Ω, while that of the electrode modified by JACM/CeO_2NPs/CS is only about 200 Ω. This indicates that the electron transfer resistance of the electrode is significantly reduced after modification, which facilitates the transfer of electrons. The electrode modified by JACM/CeO_2NPs/LOD/CS has a R_{ct} value of about 500 Ω, slightly higher than that of the JACM/CeO_2NPs/CS modified electrode, indicating that the addition of the LOD layer increases the electron transfer resistance.

Since the same electrolyte was used in EIS experiments for all the three electrodes, the resistance R_L associated with the solution between the electrodes was substantially the same, which is about 100 ohms.

In addition, we also computed the CPE values of the three electrodes. The equivalent capacitance value of the CPE can be calculated according to the following formula:

$$C_d = \frac{1}{\omega^* R_{ct}} \quad (2)$$

where C_d is the equivalent capacitance value of CPE, and ω* is the corresponding angular velocity at the half dome point shown in the bode plot (see Fig. S5). Through fitting and calculation, the capacitance of the bare Au gate electrode is about 2.92×10^{-7} S Sec^n/cm^2, while that of the JACM/CeO_2NPs/CS and the JACM/CeO_2NPs/LOD/CS modified electrode is about 4.25×10^{-7} S Sec^n/cm^2 and 1.63×10^{-7} S Sec^n/cm^2, respectively.

The dynamic surface area of the sensing platform was calculated by using Randles - Sevcik equation; area was investigated utilizing cyclic voltammetric technique, 1.0 mM $K_3Fe(CN)_6$ as a test solution and 0.1 M KCl as supporting electrolyte, at different sweep rates (Nagaraj et al., 2019a,b). At T = 298 K and for a reversible process the equation is as follows:

$$I_P = (2.69 \times 10^5) n^{\frac{3}{2}} A \nu^{\frac{1}{2}} D_0^{\frac{1}{2}} C_0^* \quad (3)$$

The area of the electrode surface is signified as A, the diffusion coefficient as D_0, i.e. 7.6×10^{-6} cm^2 s^{-1}, sweeping rate as ν, and C_0^* is the concentration of $K_3Fe(CN)_6$. From the slope of the plot of I_p vs. $\nu^{1/2}$, the surface area of the bare Au electrode was found to be 0.017 cm^2 while that of the modified electrode surface area was 0.043 cm^2, increasing by 2.5 times (see Fig. S7).

3.3. H_2O_2 detection by the JACM/CeO_2NP modified SGGTs

We further applied the JACM/CeO_2NPs modified as well as the pristine SGGTs for detection of H_2O_2. Fig. S2a shows the transfer curve measured by the bare Au gate SGGT sensor in PBS solution. The Dirac point of the transfer curve was about 0.4 V with excellent bipolarity validating the reliable performance of the prepared SGGT devices. Subsequently 0.1 mM, 1 mM and 10 mM of H_2O_2 was successively added to the pristine SGGT device, and the Dirac point of the transfer curve shifted slightly to the left with the increasing concentration of H_2O_2.

According to the definition of detection limit by IUPAC, it can be known that the target concentration corresponding to the current signal with a signal-to-noise ratio greater than 3 ($I_S/I_N > 3$) can be used as the detection limit of the biosensor. Fig. 4a displays the barrow current response (I_{DS}) of the SGGT sensor with the bare Au gate to different concentration of H_2O_2 successively over time, the detection limit of which was 1 μM (see the inset of Fig. 4a, $\Delta I_S/\Delta I_N = 0.50/0.08 > 3$).

Next the response of the SGGT sensor with the JACM/CeO_2NPs/CS modified gate to the different concentrations of H_2O_2 was measured for comparison. The transfer curves of the JACM/CeO_2NPs/CS modified SGGT sensor in response to 0.1 mM, 1 mM and 10 mM of H_2O_2 is shown in Fig. S2b. Again the transfer curves shifted horizontally to the left, but with a significantly larger amplitude than that of the SGGT with the bare Au gate. Fig. 4b shows the channel current response (I_{DS}) of the JACM/CeO_2NPs/CS modified SGGT sensor at V_G = + 0.7 V and

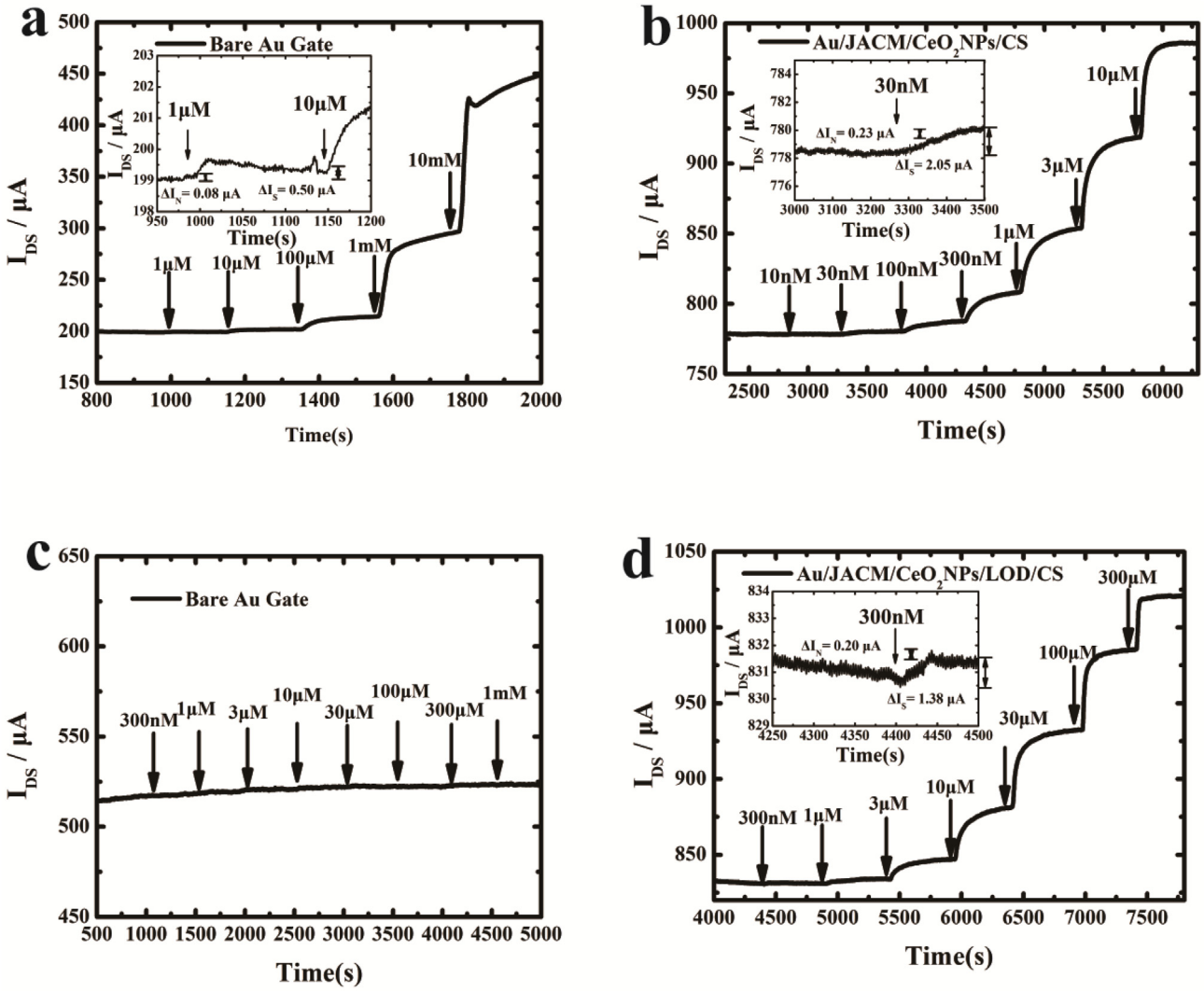

Fig. 4. The channel current responses of the SGGT with a bare Au gate (a) and a Au/JACM/CeO_2NPs/CS gate (b) to the increasing H_2O_2 concentration in PBS solution measured at V_{DS} = 0.05 V and V_G = + 0.7 V. The channel current responses of the SGGT with a bare Au gate (c) and a Au/JACM/CeO_2NPs/LOD/CS gate (d) to the increasing lactic acid concentration in PBS solution measured at V_{DS} = 0.05 V and V_G = + 0.7 V.

V_{DS} = 0.05 V with the addition of H_2O_2 at different concentrations. The inset of Fig. 4b indicates that the detection limit of the modified SGGT sensors for H_2O_2 was 30 nM ($\Delta I_S/\Delta I_N$ = 2.05 μA/0.23 μA > 3). Moreover, the increasing amplitude of current with increasing H_2O_2 concentration was much larger than that of the bare Au gate SGGT sensor. These observations confirmed that the modification of JACM/CeO_2NPs/CS effectively improved the detection performance of the SGGT sensor for H_2O_2.

3.4. Lactic acid detection by SGGTs

The SGGT devices were further applied for detection of lactic acid and the results are presented in Fig. 4. As shown in Fig. S2c, the transfer curve measured by the bare Au gate SGGT sensor for the addition of different concentrations of lactic acid (0.1 mM, 1 mM, and 10 mM respectively) in PBS solution showed good bipolarity behavior. Besides we found that the Dirac point of the transfer curve moved slightly to the left with the increase of the concentration of lactic acid. Fig. 4c shows the channel current response I_{DS} of the bare Au gate SGGT sensor when different concentrations of lactic acid were added to PBS solution successively. It can be seen from the figure the bare Au gate SGGT sensor had minimum current response to lactic acid at low concentration. This indicates that lactic acid did not spontaneously participate in electrochemical reactions on the electrode surface. As a comparison, the transfer curves of the JACM/CeO_2NPs/LOD/CS modified SGGT sensors to lactic acid also presented good bipolar behavior, but with a much larger shift to the left with increasing concentration of lactic acid (Fig. S2d).

Furthermore, the channel current I_{DS} of the modified SGGT sensor clearly showed a positive linear relation with the increasing concentration of lactic acid. The inset of Fig. 4d indicates that the detection limit of the modified SGGT sensor to lactic acid was 300 nM ($\Delta I_S/\Delta I_N$ = 1.38 μA/0.20 μA > 3).

The current response is attributed to the change of the effective gate voltage (ΔV_G^{eff}) induced by the electrochemical reaction of lactic acid on the gate electrode. Therefore, ΔV_G^{eff} is calculated by subtracting the initial gate voltage value from to the current responses at corresponding lactic acid concentrations in Fig. 4b and d and the results are plotted in Fig. 5a. And the effective voltage change can be fitted with the equation (Zhang et al., 2014, 2015):

$$V_G^{eff} = (1+\gamma)V_{E-C} = 2.30(1+\gamma)\frac{\kappa T}{2q}\log[C_{LA}] + C^{**} = \alpha \log[C_{LA}] + C^{**} \quad (4)$$

where C^{**} is constant, α = 2.30 (1 + γ) κT/2q is the slope of V_G^{eff} per decade of the lactic acid concentration, and $[C_{LA}]$ is the concentration

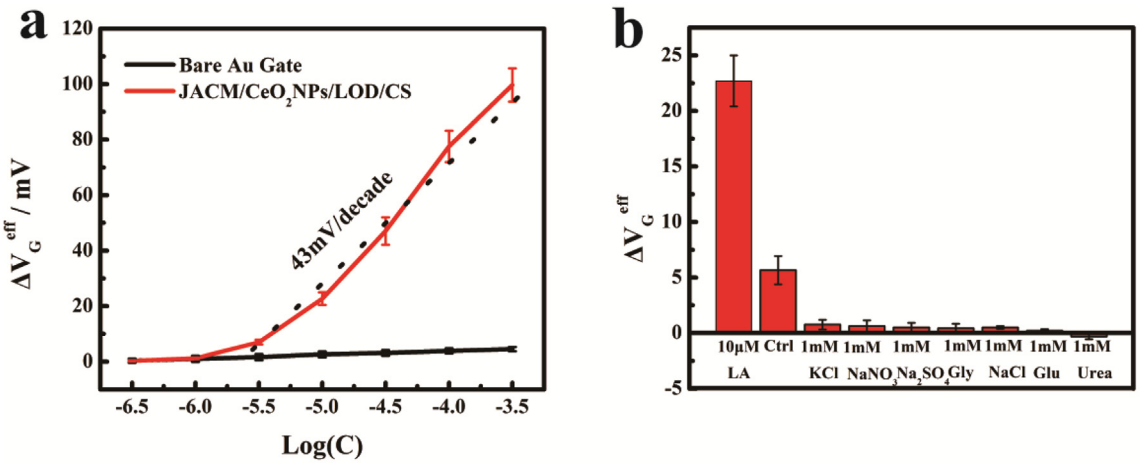

Fig. 5. (a) Effective gate voltage change (ΔV_G^{eff}) of the SGGT with a bare Au gate and Au/JACM/CeO_2NPs/LOD/CS gate versus the logarithmic value of lactic acid concentration. (b) Selectivity measurements of the SGGT device with a Au/JACM/CeO_2NPs/LOD/CS gate. The ΔV_G^{eff} signal of the device in response to the target lactic acid (10 μM) or other nontarget analytes, i.e. blank cell culture medium, K^+ (1 mM), NO_3^- (1 mM), SO_4^{2-} (1 mM), Gly (1 mM), Na^+ (1 mM), Glu (1 mM), Urea (1 mM) were compared. Error bars represent standard deviations from three independent measurements.

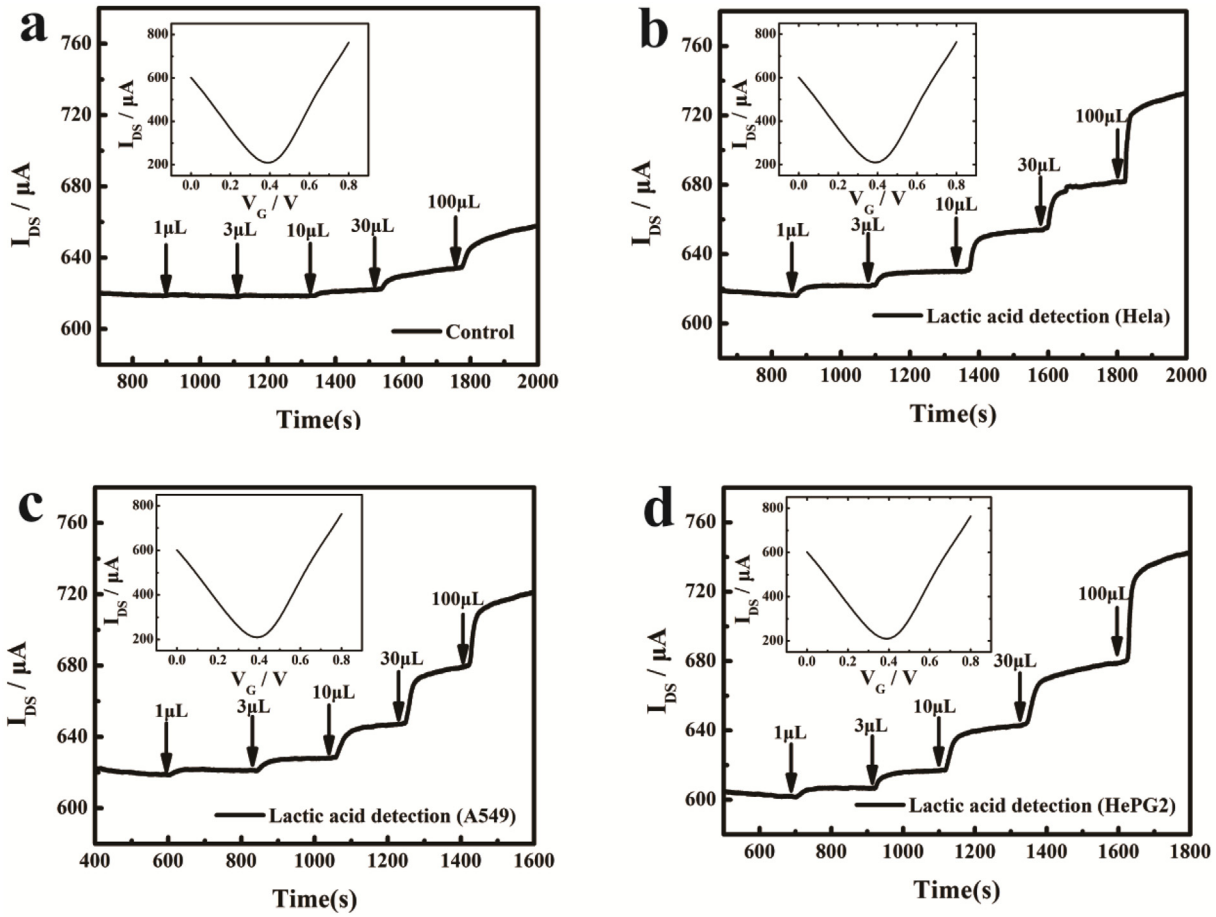

Fig. 6. Channel current responses of the SGGT with a Au/JACM/CeO_2NPs/LOD/CS gate characterized in PBS solution before and after the additions of (a) control cell culture medium (b) Hela (c) A549 (d) HepG2 of different volumes. Inset: transfer curve of the SGGT measured in PBS solution.

of lactic acid. It can be seen from Eq. (4) that the concentration of lactic acid has the effect for adjusting the effective gate voltage (V_G^{eff}) and V_G^{eff} shifts to larger values with the increasing concentration of lactic acid when $V_G = 0.7 > V_{Dirac}$ (Bernards and Malliaras, 2007; Bernards et al., 2008; Cicoira et al., 2010; Lin et al., 2010, 2011).

As shown in Fig. 5a, ΔV_G^{eff} of the unmodified and modified SGGT sensors vs. Log [lactic acid] showed a linear relationship. The slope of the modified SGGT sensor was 43 mV/decade, much larger than that of the unmodified one, and the linear range was between 3 μM and 300 μM.

The stability of the SGGT-based lactic acid sensor was also tested. Essentially, we measured the 10 μM lactic acid in PBS buffer for 10 days. The modified SGGT device was kept at 4 °C with appropriate moisture after each measurement. From the experimental results (Fig.

S6), we found that the device retains most of its performance even in one week and the half-life of the lactate oxidase modified on the electrode is roughly 10 days.

3.5. Specificity test

There may be some interference for the SGGT sensor in the detection of lactic acid in the cytoplasm, and we selected blank cell culture medium, KCl (1 mM), $NaNO_3$ (1 mM), Na_2SO_4 (1 mM), Gly (1 mM), NaCl (1 mM), Glu (1 mM), urea (1 mM) for specificity test. As shown in Fig. 5b, the modified SGGT sensor showed the most obvious response to 10 μM lactic acid (22.70 ± 2.31 mV), followed by blank cell culture medium (5.66 ± 1.28 mV). The responses of the device to other substances at a much higher concentration (1 mM) were very weak: KCl (0.76 ± 0.43 mV), $NaNO_3$ (0.63 ± 0.51 mV), Na_2SO_4 (0.51 ± 0.43 mV), Gly (0.44 ± 0.41 mV), NaCl (0.50 ± 0.12 mV), Glu (0.22 ± 0.14 mV), urea (- 0.31 ± 0.26 mV). Therefore, these substances will not affect the test results in lactic acid detection in real samples, as long as the weak influence of blank cell culture medium in the overall response is removed.

3.6. Real sample detection

The SGGT sensor with the JACM/CeO_2NPs/LOD/CS modified Au gate was finally applied for tumor cell detection based on lactic acid concentration in cell cultures. First, we cultured tumor cell lines such as HepG2, A549 and Hela. Before actual sample test, the modified SGGT sensor was calibrated with the standard curve of lactic acid concentration obtained in PBS buffer (Fig. 5a). The cell culture medium was then sampled and detected. As shown in Fig. 6b, c and d, the modified SGGT sensor showed relatively large channel current response I_{DS} to the Hela, A549 and HepG2 culture medium (diluted 1000 times) by adding successive volumes.

When tumor cells grow in medium, they metabolize glucose through the glycolysis pathway, generating significant amount of lactic acid. As shown in Fig. 3b, the lactic acid molecules first enter the LOD/CS layer of the gate electrode and are converted to H_2O_2 (1:1). The generated H_2O_2 molecules then diffuse into the underlying JACM/CeO_2NPs/CS layer and electrocatalytically converted to O_2 (1:1). This process transfers two electrons to the gate electrode and changes the effective gate potential accordingly. The small change in the effective gate potential is amplified by the transistor effect, reflecting in the large change in the channel current. We also confirm that the SGGT-based lactic acid sensor showed minimal signals to other common analytes existing in cell cultures. Therefore, we first obtained a standard curve of lactic acid concentration for the SGGT-based lactic acid sensor in PBS buffer by determining the effective gate voltage (ΔV_G^{eff}) change (from the corresponding current change) vs. the lactic acid concentration (Log (C)) as shown in Fig. 5a. The lactic acid concentration in the real sample analysis was calculated by substituting the corresponding effective gate voltage change into the standard curve (Xiong et al., 2018).

The detection result of the blank cell culture was used as control (Fig. 6a) and the actual concentration of lactic acid in the HepG2, A549 and Hela cell cultures was obtained by comparison with the standard curve of lactic acid. As shown in Table. S2, the concentration of lactic acid in HepG2 culture was 9.26 ± 0.30 mM, the concentration of lactic acid in A549 culture was 5.97 ± 0.28 mM, and the concentration of lactic acid in Hela culture was 7.50 ± 0.31 mM. This is consistent with the level of lactic acid in tumor cell cultures measured using the lactate kit.

4. Conclusion

In this paper, we first report a simple “one-step” and sustainable approach for synthesis of nanoceria loaded porous carbon (JACM/CeO_2NPs) through *in situ* pyrolysis of cerium nitrate pretreated Jerusalem artichoke stalk. The JACM/CeO_2NPs nanocomposites exhibited superior electrocatalytic performance and were applied to the functionalization of the gate electrode of solution-gated graphene transistors (SGGTs), showing a detection limit as low as 30 nM of H_2O_2. Then a miniaturized biosensor was constructed by further modifying the gate electrode with lactate oxidase for real-time detection of lactic acid, with a detection limit of 300 nM and a linear range of 3–300 μM. The subsequent selectivity test demonstrated that the SGGT-based lactic acid sensor specifically detected lactic acid even in a complex system. Finally, the lactic acid sensor was successfully applied to the determination of lactic acid content in real medium samples of cancer and normal cell cultures with high accuracy. Considering its high biocompatibility and accuracy in cell culture samples, we believe that the SGGT-based lactic acid sensor shows great potential for identifying tumor microenvironment. Currently the SGGT-based lactic acid sensor still requires power supplying and current reading from external sourcemeters, which limits its application in various circumstances. The future work would be the construction of integrated and portable SGGT-based lactic acid sensors for on-site rapid identification of tumor tissues in live animals.

Declaration of interests

The authors declare that they have no known competing financial interests or personal relationships that could have appeared to influence the work reported in this paper.

CRediT authorship contribution statement

Yulong Bi: Investigation, Validation, Writing - original draft, Writing - review & editing. **Lihui Ye:** Investigation, Writing - original draft. **Yu Mao:** Validation, Data curation. **Lu Wang:** Conceptualization, Methodology, Resources, Funding acquisition. **Hao Qu:** Conceptualization, Formal analysis, Writing - review & editing, Funding acquisition. **Jian Liu:** Methodology, Resources, Supervision. **Lei Zheng:** Resources, Supervision, Project administration.

Acknowledgments

This study was supported by the National Natural Science Foundation of China (21705031), the Natural Science Foundation of Anhui Province (1808085QB39, 1708085QC66), the Fundamental Research Funds for the Central Universities (PA2019GDQT0018, JZ2018HGTA0212), and Engineering Research Center of Bio-process by Ministry of Education in Hefei University of Technology.

Appendix A. Supplementary data

Supplementary data related to this article can be found at https://doi.org/10.1016/j.bios.2019.04.039.

References

Bêche, E., Charvin, P., Perarnau, D., 2008. Surf. Interface Anal. 40, 264–267.
Bernards, D.A., Malliaras, G.G., 2007. Adv. Funct. Mater. 17, 3538–3544.
Bernards, D.A., Macaya, D.J., Nikolou, M., DeFranco, J.A., Takamatsu, S., Malliaras, G.G., 2008. J. Mater. Chem. 18, 116–120.
Chao, M., Wu, H., Jin, K., Li, B., Wu, J.J., Zhang, G.Q., Yang, G., Hu, X., 2016. eLife 5, e15691.
Chen, Y.Z., Zhang, R., Jiao, L., Jiang, H.L., 2018. Coord. Chem. Rev. 362, 1–23.
Chen, H., Wang, J.M., Zhao, Y.L., Zhang, J.Q., Cao, C.N., 2005. Solid State Electrochem 9, 421–428.
Cicoira, F., Sessolo, M., Yaghmazadeh, O., DeFranco, J.A., Yang, S.Y., Malliaras, G.G., 2010. Adv. Mater. 22, 1012–1016.
Deshpande, S., Patil, S., Kuchibhatla, S.V.N.T., 2005. Appl. Phys. Lett. 87, 133113.
Ferrari, A.C., 2007. Solid State Commun. 143, 47–57.
Gaddam, R.R., Yang, D.F., Narayan, R., Raju, K.V.S.N., Kumar, N.A., Zhao, X.S., 2016. Nano Energy 26, 346–352.
GBD 2016 Disease and Injury Incidence and Prevalence Collaborators, 2017. Lancet 481

(390), 1151–1210.
Hammock, M.L., Knopfmacher, O., Naab, B.D., Tok, J.B.H., Bao, Z.A., 2013. ACS 483 Nano 7, 3970–3980.
Han, C., Wang, S., Wang, J., Li, M., Deng, J., Li, H., Wang, Y., 2014. Nano Res 7 (485), 1809–1819.
Hernández-Ibáñez, N., García-Cruz, L., Montiel, V., 2016. Biosens. Bioelectron. 77, 1168–1174.
Hou, J.H., Cao, C.B., Idrees, F., Ma, X.L., 2015. ACS Nano 9, 2556–2564.
Huang, H., Lovell, J.F., 2016. Adv. Funct. Mater. 27, 1603524.
Khodagholy, D., Curto, V.F., Fraser, K.J., 2012. J. Mater. Chem. 22, 4440–4443.
Lei, Y.U., Chen, T.U., Luo, Y., 2015. Front. Environ. Sci. Eng. China 9, 206–215.
Lin, P., Yan, F., 2012. Adv. Mater. 24, 34–51.
Lin, P., Luo, X.T., Hsing, I.M., Yan, F., 2011. Adv. Mater. 23, 4035–4040.
Lin, P., Yan, F., Yu, J.J., Chan, H.L.W., Yang, M., 2010. Adv. Mater. 22, 3655–3660.
Liu, B.W., Sun, Z.Y., Huang, P.J., Liu, J.W., 2015. J. Am. Chem. Soc. 137, 1290–1295.
Liu, Y.X., Dong, X.C., Chen, P., 2012. Chem. Soc. Rev. 41, 2283–2307.
Long, X.H., Shao, H.B., Ling, L., Liu, L.P., Liu, Z.P., 2016. Renew. Sustain. Energy Rev. 54, 1382–1388.
Miao, P., Tang, Y., Wang, L., 2017. ACS Appl. Mater. Interfaces 9, 3940–3947.
Montini, T., Melchionna, M., Monai, M., 2016. Chem. Rev. 116, 5987–6041.
Nagaraj, P.S., Shweta, J.M., Sharanappa, T.N., 2015. Analytical Methods 7, 8673–8682.
Nagaraj, P.S., Deepti, S.N., Shweta, J.M., Raghava, R.K., Shyam, S.S., Tejraj, M.A., 2019a. Anal. Chim. Acta 1051, 58–72.
Nagaraj, P.S., Deepti, S.N., Shweta, J.M., Raghava, R.K., Shyam, S.S., Tejraj, M.A., 2019b. Colloids Surfaces B Biointerfaces 177, 407–415.
Novoselov, K.S., Geim, A.K., Morozov, S.V., Jiang, D., Zhang, Y., Dubonos, S.V., Grigorieva, I.V., Firsov, A.A., 2004. Science 306, 666.
Pode, R., 2016. Renew. Sustain. Energy Rev. 53, 1468–1485.
Ross, M.J., Öberg, J., Brené, S., 2010. Proc. Natl. Acad. Sci. U.S.A. 107, 20087–20092.
Rumyantsev, S., Liu, G., Shur, M.S., Potyrailo, R.A., Balandin, A.A., 2012. Nano Lett. 12, 2294–2298.
Saikat, D., Asim, B., Kevin, C.W.W., 2014. Energy Environ. Sci. 7, 3574–3592.
Shan, C.S., Yang, H.F., Han, D.X., Zhang, Q.X., Ivaska, A., Niu, L., 2010. Biosens. Bioelectron. 25, 1070–1074.
Tserng, K.Y., Gilfillan, C.A., Kalhan, S.C., 1984. Anal. Chem. 56, 517–523.
Veerakumar, P., Veeramani, V., Chen, S.M., Madhu, R., Liu, S.B., 2016. ACS Appl. Mater. Interfaces 8, 1319–1326.
Wang, X.J., Feng, J., Bai, Y.C., Zhang, Q., Yin, Y.D., 2016. Chem. Rev. 116, 10983–11060.
Xiong, C., Zhang, T.F., Kong, W.Y., Zhang, Z.X., Qu, H., Chen, W., Luo, L.B., Zheng, L., 2018. Biosens. Bioelectron. 101, 21–28.
Xie, J.S., Wu, H., Dai, C.Y., Pan, Q.R., Ding, Z.H., Hu, D.Q., Ji, B.Y., Luo, Y., Hu, X., 2014. Sci. Rep. 4, 1–12.
Zhai, D.Y., Liu, B.R., Shi, Y., Pan, L.J., Wang, Y.Q., Li, W.B., Zhang, R., Yu, G.H., 2013. ACS Nano 7, 3540–3546.
Zhang, M., Liao, C.Z., Mak, C.H., You, P., Mak, C.L., Yan, F., 2015. Sci. Rep. 5, 8311.
Zhang, M., Liao, C.Z., Yao, Y., Liu, Z.K., Gong, F.F., Yan, F., 2014. Adv. Funct. Mater. 24, 978–985.
Zhang, Y., Wu, C.Y., Zhou, X.J., Wu, X.C., Yang, Y.Q., Wu, H.X., Guo, S.W., Zhang, J.Y., 2013. Nanoscale 5, 1816–1819.
Zhang, Z., Zhao, H., Teng, Y., 2017. Adv. Energy Mater. 8, 1700174.
Zheng, W.L., Teng, J., Cheng, L., Ye, Y.W., Pan, D.D., Wu, J.J., Xue, F., Liu, G.D., Chen, W., 2016. Biosens. Bioelectron. 80, 574–581.
Zhong, S.L., Zhuang, J.Y., Yang, D.P., Tang, D.P., 2017. Biosens. Bioelectron. 96, 26–32.
Zhou, X., Wang, P., Zhang, Y., Wang, L., Zhang, L., Zhang, L., Xu, L., Liu, L., 2017. J. Mater. Chem. 5, 12958–12968.
Zhou, Z., Hartmann, M., 2013. Chem. Soc. Rev. 42, 3894–3912.